Check for updates

doi.org/10.1002/batt.202000201

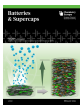

Architecture Transformations of Ultrahigh Areal Capacity Air Cathodes for Lithium-Oxygen Batteries

Louisa C. Greenburg,[a] Christian O. Plaza-Rivera,[a] Jae-Woo Kim,[b] John W. Connell,*[c] and Yi Lin*[b]

Lithium-oxygen ($Li–O_2$) batteries have the highest known theoretical energy density but are still not practical for use in most applications. A key aspect that has been largely overlooked in the field is how to improve the reversible areal capacity of the air cathode to a competitive level (> 5–10 mAh cm^{-2}). For carbon-based air cathodes, increase of areal capacity requires a corresponding increase of carbon mass loading. As a result, the electrode thickness also increases which impedes the mass transport of Li ions and O_2 needed for battery reactions. It is therefore imperative to investigate not only the air cathode composition, but also its dimensional architecture, for the effective function of high areal capacity $Li–O_2$ batteries. Herein, we present the use of several representative additives of carbon-based nanomaterials, including carbon black, two different diameters of multi-walled carbon nanotubes, and graphene materials from two sources, into a high mass loading (10 mg cm^{-2}), ultrathick (~100 μm) air cathode architectural platform matrix based on dry-compressed holey graphene. The performances of these all-carbon composite air cathodes differ from that of the neat holey graphene, but not by a simple addition or subtraction effect. In addition, the additive effects to full discharge and curtailed cycling experiments are significantly different. The presented results strongly suggest that the architectural volume expandability is critical for the full discharge properties. However, the cycling performance depends more upon the resilience of the air cathode architecture ("breathability"), which does not necessarily correlate with its expandability.

1. Introduction

Lithium-oxygen ($Li–O_2$) batteries are a unique, attractive, high energy density battery platform because presumably the cathode reagent, O_2, is limitlessly obtained from an external atmosphere.[1] Substantial progress has been made in this field during the past decade or so, especially with regard to the electrochemical reaction mechanism of the battery[2] and various cathode catalytic systems that facilitate discharge and charge reactions.[3] However, $Li–O_2$ batteries are still far from practical due to a variety of formidable challenges including, for example, the low reversible capacity, limited rate performance, and various parasitic reactions such as those related to the perceived applications directly in ambient air.[4]

High surface area carbon nanomaterials such as carbon black, carbon nanotubes, and graphene have been top choices as the air cathode materials due to their excellent electrical conductivity and highly electrochemically accessible surface area.[5] The past research in $Li–O_2$ battery air cathodes has been predominantly focused on *how and which* electrode constituents, such as these high surface area carbons as well as the associated catalysts, can enhance the battery reactions.[1–3] Specific capacity of the air cathodes with regard to the carbon mass (C_{m-C}, in mAh g_C^{-1}) has been a critical parameter studied to evaluate the performance of carbon-based systems. However, because carbon is the host material but not the active one, the reported specific capacity values can be misleading because it does not fully reflect the practical efficacy of the air cathode especially when only a minuscule amount of carbon is used. For example, full specific capacity values of carbon-based air cathodes, including those incorporated with catalysts, are mostly reported in the range of 3,000–20,000 mAh g_C^{-1}.[1,3] Yet, because the carbon mass loading (m_{A-C}) is often low (typically 0.1–0.5 mg cm^{-2}), the full capacities in terms of geometrical electrode area (areal capacity, C_A, in mAh cm^{-2}) rarely exceed 2 mAh cm^{-2}. In addition, since most $Li–O_2$ batteries do not cycle well when subjected to 100% depth of discharge (DOD), it has been common to cycle a $Li–O_2$ battery at a curtailed specific capacity, typically 500–1000 mAh g_C^{-1}. This translates to even lower areal capacity values (< 0.1–0.5 mAh cm^{-2}), far from competitive when comparing to those of the state-of-the-art Li-ion batteries (2–4 mAh cm^{-2} in cycling capacity).[6]

Consequently, besides "*how and which*", it is imperative to also investigate *how much* discharge product can be effectively held within the electrode scaffold without failure. Although carbon is not the active cathode reagent, it generally dictates the amount of surface and volume available for the growth of

[a] *L. C. Greenburg, C. O. Plaza-Rivera*
NASA Interns, Fellows, and Scholars (NIFS) Program
NASA Langley Research Center
Hampton, VA 23681-2199, USA
[b] *Dr. J.-W. Kim, Dr. Y. Lin*
National Institute of Aerospace
100 Exploration Way, Hampton, VA 23666-6147, USA
E-mail: yi.lin-1@nasa.gov
[c] *Dr. J. W. Connell*
Advanced Materials and Processing Branch
NASA Langley Research Center
Hampton, VA 23681-2199, USA
E-mail: john.w.connell@nasa.gov

Supporting information for this article is available on the WWW under https://doi.org/10.1002/batt.202000201

© 2020 Wiley-VCH GmbH

solid discharge products. Therefore, the areal capacity of the air cathode is directly related to the available carbon mass loading. For instance, in order to achieve a cyclable areal capacity of 5 mAh cm^{-2} with a curtailed specific capacity of 1000 mAh g_C^{-1}, the carbon mass loading needs to be at 5 mg cm^{-2}, much higher than what is normal in the literature as stated above. Besides considerations in parasitic reactions stemming from the carbon itself,[5,7] a major concern over increasing carbon mass loading is the increase of air cathode thickness, which makes the discharge and charge reactions more sluggish due to reduced mass transport efficiency (e.g., Li ions, O_2, and soluble catalytic species). Therefore, both material composition and dimensional architecture constitution of the air cathode are critical in order to allow the battery reaction to proceed at desired rates and efficiency, especially at much increased carbon mass loadings. Only recently, a few reports have emerged (mostly since 2017) that have emphasized carbon mass loading and areal capacity of the air cathode in Li–O_2 batteries.[8–20]

We recently developed a versatile, high carbon mass loading air cathode architectural platform based on dry-pressed holey graphene (hG).[9] The unique compressibility of hG, enabled by the presence of through-thickness holes on the graphene sheets,[21] allows the facile dry-press preparation of high performance air cathodes without the need of solvent or binder.[9,10] High carbon mass loadings can be simply achieved by adding more hG powder to the pressing die. In addition, hG can also be used as a compressible matrix to host catalyst materials in the porous architecture for enhanced air cathode performance with a high areal capacity.[10a] With the additional benefit from the enhanced ion transport provided by the nanometer-sized holes on the hG sheets,[22] the hG-based air cathode architectures are a nearly ideal platform in both serving as an effective electrical scaffold and providing sufficient electrochemically accessible surfaces and voids. Even at a carbon mass loading as high as 10 mg cm^{-2}, neat hG air cathodes retained excellent gravimetric performance in a full discharge, ~4000 mAh g_C^{-1} at 0.2 mA cm^{-2}, corresponding to an ultrahigh areal capacity of 40 mAh cm^{-2}.[28] Such air cathodes were run under a curtailed reversible capacity of 2 mAh cm^{-2} at the same current density for over 20 cycles,[28] and can be improved to ~50 cycles when lithium iodide is applied as a redox mediator.[10b] While these numbers are among the highest available in the literature, much more improvement in reversible capacity and cyclability is still needed for these air cathodes to be practically meaningful.

In this report, we take a further look into the importance of electrode architecture to the performance of high areal capacity air cathodes. Building on the previous success in the high mass loading hG-based architectural platform, we herein discuss the effect of various carbon nanomaterial additives into this platform on both the full discharge capacity and the cyclability of the resultant Li–O_2 batteries. It is shown that there is no simple addition or reduction effect from adding any of these carbon nanomaterial fillers. Rather, the remarkable different consequences in full discharge and cycling performances could be attributed to the different enhancement or disruption effects of the all-carbon air cathode architectures from the various structural characteristics of the additives.

2. Results and Discussion

2.1. hG-Based All-Carbon Composite Air Cathodes

The five different carbon nanomaterial additives selected can be divided into three categories by their dimensionalities (Scheme 1): (1) 0-dimensional (0D): carbon black (CB; commonly used as a conductive additive for electrode preparations); (2) 1-dimensional (1D): multiwalled carbon nanotubes (MWNTs) with two different diameter ranges: "small" (MWNT-S; diameter <8 nm as labeled) and "large" (MWNT-L; diameter ~20–150 nm as labeled); and (3) 2-dimensional (2D): chemically reduced graphene oxide (c-G; often referred to as "rGO", from chemical reduction) and as-received graphene that has been used as the hG precursor in our laboratory (t-G; from thermal reduction/exfoliation). These carbon nanomaterial additives are all in the form of black-colored powders (Figure S1). t-G is an exceptionally lightweight powder, while all the other carbon additive powders, including c-G, are comparably much denser. The host material hG, from a single-step thermal air oxidation of t-G,[23] exhibits similar but slightly lower apparent density than t-G as a result from weight reduction (hole formation) but with largely retained occupied volume.

Scanning electron microscopy (SEM) images of these carbon nanomaterials and hG are provided in Figure S2. The CB sample consists of nanoparticles with average sizes of ~50–100 nm. MWNT-L consists of nanotubes with diameters in the range of tens to over 100 nm, while MWNT-S consists of bundles of much thinner nanotubes with individual nanotube diameters <10 nm. Both c-G and t-G samples are extremely thin (<10 atomic layers) reduced graphene oxide sheets, but with distinctively different morphology. c-G sheet surfaces appear rather smooth, while t-G sheets are considerably more "wrinkled". From a lower magnification (Figures S2g & h), c-G particles are mostly stacked assemblies, while t-G particles exhibit much less tendency to re-stack. Such difference is directly reflected in their apparent densities (Figure S1) and may be readily attributed to their different processing conditions during reduction: liquid phase chemical reduction for c-G[24] vs. gas phase thermal reduction for t-G (accompanied by graphene exfoliation due to rapidly released gaseous side products).[25] hG sheets are of similar morphology as the precursor material t-G, except for the presence of arrays of holes through the sheet thickness with hole diameters in the typical range of 5–20 nm (Figure S2a).[23]

All five types of additives were mixed with hG in a weight ratio of 1:5 unless otherwise specified. The mixing was conducted with a mechanical ball-mill, but a short duration (10 s) was used to prevent undesirable pre-densification of the hG matrix. The composite powder mixtures were subsequently pressed into free-standing (for physical characterizations) or mesh-reinforced discs (as air cathodes for Li–O_2 battery tests[9,10]) without any solvent or binder. Unlike hG or hG-based

© 2020 Wiley-VCH GmbH

25666223, 2021, 1, Downloaded from https://chemistry-europe.onlinelibrary.wiley.com/doi/10.1002/batt.202000201 by University of Ulsan, Wiley Online Library on [11/11/2025]. See the Terms and Conditions (https://onlinelibrary.wiley.com/terms-and-conditions) on Wiley Online Library for rules of use; OA articles are governed by the applicable Creative Commons License

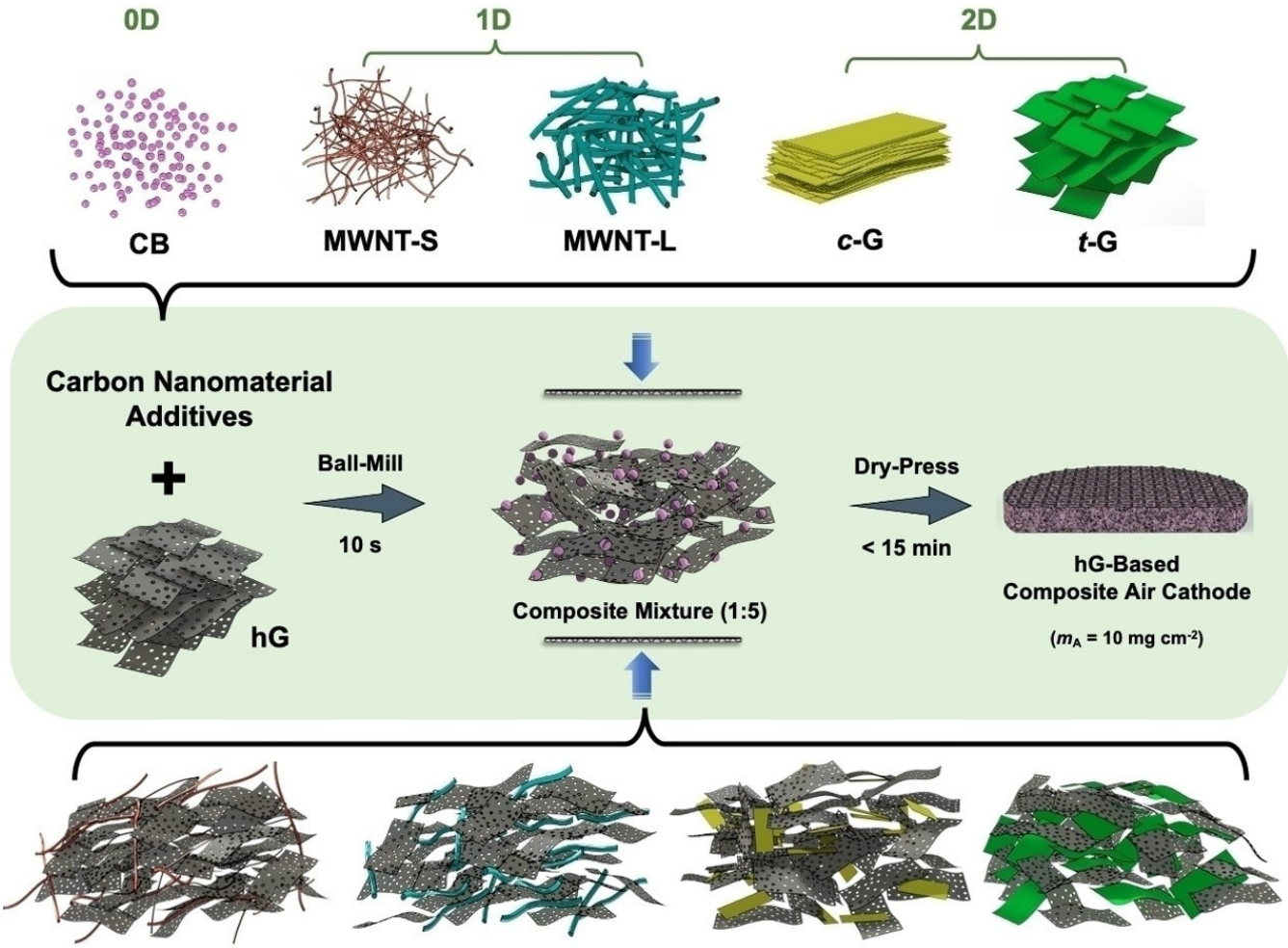

Scheme 1. Schematics on the facile, solvent-free, and binder-free procedure in the preparation of composite mixtures by adding various carbon nanomaterial additives (CB, MWNT-S, MWNT-L, c-G, and t-G) to hG host (1 : 5 in weight), followed by dry-pressing the mixtures into the corresponding composite air cathodes.

composites, the articles from dry pressing the additive powders by themselves without hG were all weakly bound (loose and/or brittle) and could not form robust discs. Since all the additives and the hG host are different allotropes of carbon, the composite discs are "all-carbon". The total carbon mass loadings (m_{A-C}, including both hG and the respective additive) for all discs in this study were ~10 mg cm^{-2}. The entire process to prepare such high mass loading discs, including both mixing and pressing, could be completed well within an hour. In comparison, the solvent-based slurry or filtration approaches for electrode preparation would take much longer to complete with extended periods needed for processing and solvent removal.[26] It should also be noted that there have been several reports on composite carbon nanomaterial-based air cathodes based on both graphene and carbon nanotubes.[27] However, the air cathode mass loadings were all in the range of 0.3–0.5 mg cm^{-2}, while our work herein discusses the performance at ultrahigh carbon mass loading (10 mg cm^{-2}) using a different electrode preparation technique (solvent-free mix-and-press) and thus shares little similarity.

Cross-sectional SEM images of the as-prepared discs (Figure 1) show that the additives are all well distributed throughout the hG matrix. The short mixing duration (10 s) with ball-mill has been previously proven sufficient to prepare homogeneous mixtures of various powdery additives with hG matrix,[10,28] which may be attributed to the extremely loosely packed hG sheets that allow for the facile penetration of additives in the absence of solvents. Quantitative characterization results of all the composite discs and the neat hG disc are summarized in Table 1. Among all the additives, only c-G resulted in higher composite disc density than the neat hG disc itself under the same pressing conditions. This is likely due to the smooth and compact sheet morphology of c-G coupled with the dimensional similarity between c-G and hG (i.e., both are reduced graphene sheets but via different means), resulting in stronger filler-matrix interactions. t-G, however, resulted in the lowest composite disc density, which may be readily attributed to the highly resilient ("wrinkled") nature of the thermally exfoliated graphene sheets. Consistently, our previous results have shown that neat t-G discs from similar dry

© 2020 Wiley-VCH GmbH

25666223, 2021, 1, Downloaded from https://chemistry-europe.onlinelibrary.wiley.com/doi/10.1002/batt.202000201 by University of Ulsan, Wiley Online Library on [11/11/2025]. See the Terms and Conditions (https://onlinelibrary.wiley.com/terms-and-conditions) on Wiley Online Library for rules of use; OA articles are governed by the applicable Creative Commons License

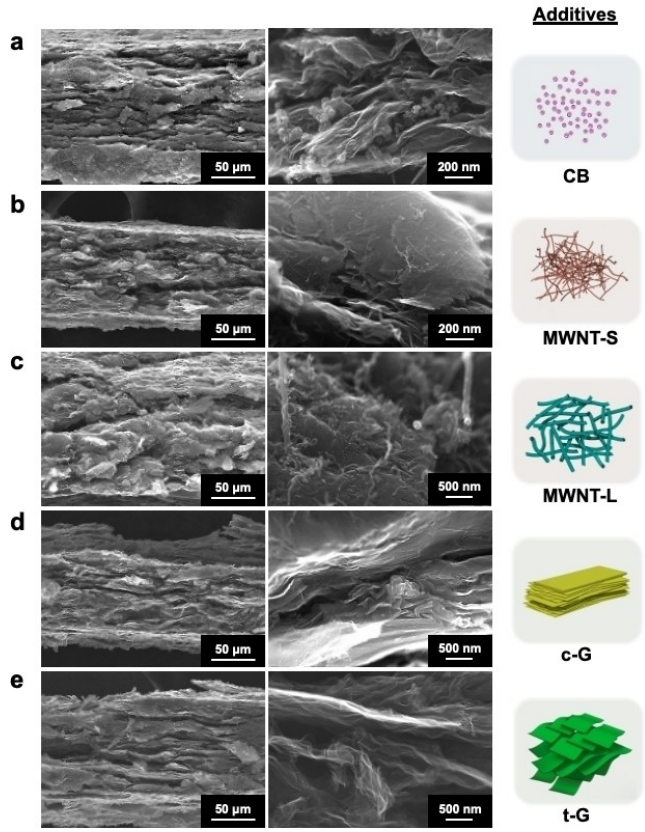

Figure 1. SEM cross-sections of dry-pressed hG composite discs with various carbon nanomaterial additives: a) CB; b) MWNT-S; c) MWNT-L; d) c-G; and e) t-G at lower (left column) and higher magnifications (right column).

compression are weakly bound due to spontaneous volume/thickness rebound upon release of the compression pressure.[21]

The density values of the composite discs do not directly correlate with the Brunauer-Emmett-Teller (BET) surface area values (Table 1). More specifically, the uses of CB and c-G both resulted in ~30% decrease in surface area values, while other additives had little effect. All additives appear to have disrupted the conductive network of the hG itself, with all composite discs exhibiting lower surface conductivity values than the neat hG disc. Among them, the MWNT-L/hG disc had the lowest conductivity value of 185 S cm^{-1}, 38% less than the neat hG disc (296 S cm^{-1}). C/O atomic ratios measured with X-ray photoelectron spectroscopy (XPS) were in a consistent range of 10–20, suggesting that all the discs consist of slightly oxidized carbon (see Table S1 for more detailed deconvolution data). The C/O values of the neat hG disc and CB/hG are ~15, while those of MWNT-L/hG and c-G/hG were in the lower range (~10; i.e., slightly more oxidized) and those of MWNT-S/hG and t-G/hG were in the higher end (~20; i.e., slightly less oxidized). Overall, the carbon additives utilized in this work only led to some minor differences in physical and chemical properties of the composite discs compared to the neat hG disc.

It is known that metallic catalysts and heteroatomic (e.g. nitrogen, sulfur) doping with carbon may render catalytic properties for the discharge and charge reactions in Li–O_2 batteries.[3] These carbon nanomaterial additives, all commercially obtained, might contain one or more such impurities from their respective preparation processes. A short step cycle protocol was first used to examine whether such effects are prominent by using these additives. In this protocol, the Li–O_2 batteries were subjected to cycle at three different current densities (0.1, 0.2, and 0.5 mA cm^{-2}), each with just two cycles with a moderate curtailing capacity of 2 mAh cm^{-2}. As shown in Figure S3, the profiles of all the composite discs almost completely overlap at all three current densities, suggesting there is negligible difference in catalytic effect, if any, from any of these additives. Therefore, all additives may be considered catalytically equivalent toward both discharge and charge reactions for these all-carbon composite air cathodes.

2.2. Full Discharge Performance

The Li–O_2 batteries with the composite air cathodes and the neat hG air cathode were subject to full (deep) discharge at the same current density of 0.2 mA cm^{-2}. As shown in Figure 2 and Table 2, these batteries exhibited significantly different capacity values. The areal capacity of the neat hG air cathode was 47 mAh cm^{-2} (specific capacity 4376 mAh g_C^{-1}) consistent with our previous reports at the same hG mass loading (10 mg cm^{-2}).[9] With the exception of t-G, the use of all carbon nanomaterial additives resulted in reduced capacity, with the MWNT-L affording the largest decrease down to only 14 mAh cm^{-2} (or 1347 mAh g_C^{-1}). Addition of t-G, however, allowed for a slight increase to 53 mAh cm^{-2} (or 4986 mAh g_C^{-1}). The order of additive performance in the composite cathodes can be summarized as: MWNT-L < c-G < MWNT-S < CB < no

Table 1. Physical and chemical characterizations of dry-pressed hG composite discs with various carbon nanomaterial additives (additive: hG = 1:5 w/w). Data from the neat hG disc is also shown for comparison.

Additives	No additives (hG only)	CB	MWNT-S	MWNT-L	c-G	t-G
Density [g cm^{-3}]	1.11	1.01	0.91	1.00	1.18	0.85
Conductivity [S cm^{-1}]	296	201	242	185	216	274
C/O Molar ratio	15.1	15.9	18.6	10.1	9.9	19.8
BET surface area [m^2 g^{-1}]	329	223	363	359	237	314

© 2020 Wiley-VCH GmbH

25666223, 2021, 1, Downloaded from https://chemistry-europe.onlinelibrary.wiley.com/doi/10.1002/batt.202000201 by University of Ulsan, Wiley Online Library on [11/11/2025]. See the Terms and Conditions (https://onlinelibrary.wiley.com/terms-and-conditions) on Wiley Online Library for rules of use; OA articles are governed by the applicable Creative Commons License

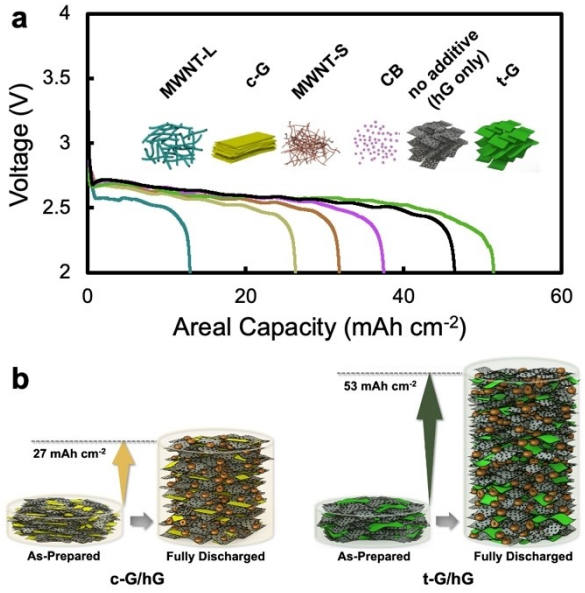

Figure 2. a) Full discharge curves of Li–O_2 batteries with dry-pressed hG composite air cathodes with various carbon nanomaterial additives (additive: hG = 1:5 w/w) in comparison to that of the neat hG air cathode. Current densities were 0.2 mA cm^{-2}. b) Cartoon illustrations (not drawn to scale) showing the different architectural volume expansions of c-G/hG vs. t-G/hG air cathode systems associated with their different full discharge areal capacities. Toroidal Li_2O_2 particles are shown in golden color.

additive (hG only) < t-G. Since all the composite air cathodes contained a dominating amount of hG and ~20 wt% of additives, the observed large variation in full discharge capacity values is far from a simple addition or subtraction effect from the hG and the additives. Only the use of CB resulted in nearly identical utilization of the hG host as the neat electrode if only the weight of hG is considered (4448 vs. 4376 mAh g_{hG}^{-1}, see Table 2). Multiple cells were fabricated and tested for each air cathode composition (Table S2). While the individual cell performance varied, the overall performance trends among different air cathode compositions are consistent with the above description.

Before proposing an explanation of the above observations, one must first be aware of the extraordinary volumetric effects that should be expected from ultrahigh areal capacity air cathodes as a result from the unique non-aqueous Li–O_2 battery chemistry. In a simplified calculation, considering Li_2O_2 as the main insoluble discharge product in a typical two-electron discharge process,[1] each mAh cm^{-2} of capacity is equivalent to 18.65 μmol cm^{-2} of Li_2O_2, or 3.7 μm in thickness – if the newly formed Li_2O_2 were a fully condensed layer (Li_2O_2 density ~2.31 g cm^{-3}). While the original disc thicknesses were all in the range of 90–130 μm at the carbon mass loading of 10 mg cm^{-2}, the formed Li_2O_2 would translate to a 196 μm in thickness increase for the 53 mAh cm^{-2} of areal capacity from the t-G/hG air cathode. In the case of high areal capacity batteries, Li_2O_2 are mostly micrometer-sized individual toroidal shaped particles attached to the carbon substrates (Figure S4). Although the hG-based air cathodes are mesoporous (i.e., high BET surface area), the voids that need to accommodate these discharge products are required to be in the micrometer scale which do not exist in the as-pressed densified air cathodes if the carbon surfaces are effectively utilized (Figure 1). Therefore, significant thickness increase of the air cathode (Δt), likely several times that of a presumed fully condensed Li_2O_2 layer, are needed to accommodate the newly formed loosely packed Li_2O_2 particles. The thickness increase Δt is defined by Equation (1):

$$\Delta t = t_D\ (\Delta V/\Delta V_0)\ C_A \quad (1)$$

where t_D is the thickness of a presumed Li_2O_2 condensed layer per unit areal capacity [3.7 μm (mAh cm^{-2})$^{-1}$]; ΔV and ΔV_0 are the actual occupied volume of formed Li_2O_2 species and the volume of a presumed Li_2O_2 condensed layer, respectively; and C_A is the areal capacity of the air cathode defined by Equation (2):

$$C_A = C_{m-C}\ m_{A-C} = C/A \quad (2)$$

where C_{m-C} is the specific capacity of the air cathode based on carbon mass, m_{A-C} is the carbon mass loading, C is the measured capacity, and A is the geometric area of the air cathode.

Air cathodes with low carbon mass loading (< 1 mg cm^{-2}) and low areal capacity (< 1 mAh cm^{-2}) as commonly reported in the literature do not experience any significant thickness change (a few micrometers or less from equations above), with the deposited discharge products mostly a surface phenomenon. In comparison, the morphology change of high mass loading, high areal capacity air cathode upon discharge is a 3-

Table 2. Full discharge properties of Li–O_2 batteries with dry-pressed hG composite air cathodes with various carbon nanomaterial additives (additive: hG = 1:5 w/w) at a current density of 0.2 mA cm^{-2}. Data from the neat hG air cathode is also shown for comparison. Specific capacity values are calculated against the total carbon mass (in mAh g_C^{-1}) and the mass of hG only (in mAh g_{hG}^{-1}) in the air electrode.

Additives		No Additives (hG only)	CB	MWNT-S	MWNT-L	c-G	t-G
Areal Capacity [mAh cm^{-2}]		47.0	38.5	32.9	13.9	27.3	53.0
Specific Capacity	per total C mass [mAh g_C^{-1}]	4376	3740	3429	1347	2602	4986
	per hG host mass [mAh g_{hG}^{-1}]	4376	4448	4114	1617	3122	5983
Half Discharge Voltage [V]		2.59	2.60	2.58	2.55	2.47	2.58

© 2020 Wiley-VCH GmbH

25666223, 2021, 1, Downloaded from https://chemistry-europe.onlinelibrary.wiley.com/doi/10.1002/batt.202000201 by University of Ulsan, Wiley Online Library on [11/11/2025]. See the Terms and Conditions (https://onlinelibrary.wiley.com/terms-and-conditions) on Wiley Online Library for rules of use; OA articles are governed by the applicable Creative Commons License

dimensional volumetric phenomenon. As shown in Figure S5, all the high mass loading air cathodes after full discharge became much thicker when compared to the as-prepared dry electrodes (~100 μm), with some into nearly millimeter range (equivalent to ~10–20% void volume utilization). With such enormous volume change, the hG-based air cathode architectures remained sustainable in the discharge process to allow not only the ready access of ions and O_2, but also the growth of a massive number of discharge products without scaffold failure. The extraordinary electrochemical sustainability against immense volume expansion of the dry-pressed hG-based air cathode system is attributed to their unique physical characteristics when wetted with electrolyte. Unlike conventional slurry-casted electrodes, the hG-based electrodes exhibited immediate swelling when applying the liquid electrolyte. The liquid electrolyte filled in-between the hG sheets and interrupted the strong inter-sheet interactions that held the disc together under dry conditions and expanded the inter-sheet distance into microscopic voids. Although the swollen air cathodes became mechanically weak, the small pressure applied during crimping process ($<$10 MPa) was sufficient to render the compressed discs highly electrochemically viable, as seen in the electrochemical impedance spectra of the various as-fabricated Li–O_2 batteries (Figure S6). These swollen hG-based air cathodes are best described as electrolyte-filled, quasi-slurry-like, microporous, and conductive architectures, which are key to accommodate the immense volume expansion.

With all the carbon nanomaterial additives chemically similar (Tables 1 and S1), we propose that the differences in the full discharge capacity values are due to the transformation of architectural expandability by these additives to accommodate the volume needed for discharge products. For example, results from the case of t-G vs. c-G as additives strongly support this concept. The use of t-G as an additive resulted in nearly two times the capacity compared to c-G (53 vs. 27 mAh cm^{-2}). This would thus require approximately two times in Δt for t-G/hG to accommodate the additional Li_2O_2 formed (Figure 2b). As mentioned previously, t-G, being the precursor material for hG but without the through-thickness holes, exhibited significant volume rebound upon releasing the pressure after dry-pressing, forming mechanically weak discs that are hard to handle ("not compressible").[21] This is due to the lack of hole-induced inter-sheet interactions that would have held a pressed disc in a condensed shape. With hG as the dominant host matrix, the as-prepared t-G/hG disc can be held in a condensed shape, but understandably exhibited the lowest density among all composite discs. The volume rebound properties from t-G and the structural similarity of t-G vs. hG therefore allowed for improvement in its expandability when filled with electrolytes while retaining the integrity of the electrochemical scaffold, resulting in higher full discharge capacity than the neat hG cathode itself. On the other hand, the other 2D additive, c-G (chemically reduced graphene, "rGO"), consists of much tighter packed exfoliated graphene sheets when in dry form, very different from the ultralightweight appearance of t-G from thermal reduction (Figures S1 & S2). Although c-G resembles hG as also being 2D, its addition to the hG host architecture resulted in disruption of the volume expandability rather than providing any improvement due to its "rigid" nature, leading to much inferior full discharge performance.

The other carbon nanomaterial fillers, which also lacked the volumetrically reboundable feature, all exhibited different levels of architectural disruption in the compressed hG host architecture. Therefore, all of them resulted in reduction in full discharge capacity. CB as a 0D filler might have had the best distribution among the hG matrix after mixing and thus had the least significant disruption effect on the architectural expandability and thus the least reduction of measured capacity. In the comparison between the two 1D fillers, MWNT-L, being of much larger diameters and lower aspect ratios than MWNT-S, may have rendered less reliable electrical percolation and architectural stability in the volume expanded air cathodes when filled with electrolytes. As shown in Figure S5b, the fully discharged MWNT-L/hG cathode exhibited visible cracks, while both CB/hG and t-G/hG air cathodes appeared smooth after full discharge, suggesting higher architectural stability of the latter electrodes under these conditions.

Consistently, it has been demonstrated that densified "hard carbon" based air cathodes that lack structural flexibility are of negligible capacity despite being "porous".[5b,c] A prime example is carbon-based gas diffusion layers, which are excellent electrode platforms for fuel cells and zinc-air batteries where the reactants and products are either soluble or gaseous. In comparison, for non-aqueous Li–O_2 batteries, as long as the discharge product is insoluble, architectural expandability for a pre-densified air cathode is required for ultrahigh areal capacity. Notably, besides our dry-pressed hG-based system, another viable system with comparable full discharge areal capacity values reported in the literature is carbon nanotube films.[12,13] The highly entangled carbon nanotube network was also shown to endure large volume expansion without structural and electrochemical failure while still allowing the accessibility of ions and O_2.[12] The MWNT additives used in this work, however, were guest fillers in the hG host architecture and do not form an entangled network, and therefore play a different (secondary) role in the air cathode function. Another option for high areal capacity air cathode platform is ultrathick architectures with a sufficient amount of pre-existing macropores such as wood-derived carbon platforms.[16] However, both mass and volume efficiencies need to be carefully considered.

For the hG-based composite air cathodes, we have yet been able to identify a plausible means to directly quantify the architectural expandability. Typical mechanical tests of dry discs are likely not relevant because the expandability is related to the state of swollen electrodes in the presence of electrolyte. Also irrelevant is data from BET surface area measurements, which provides valuable information on micropores ($<$2 nm) and mesopores (2–50 nm) for ion transport but has no meaningful contribution at such ultrahigh areal capacity considering the average size of Li_2O_2 discharge products are in the micrometer range. The relative differences in the dry disc density values of the hG composite discs (Table 1) could be an indirect measure of volume rebound after dry compression and

© 2020 Wiley-VCH GmbH

25666223, 2021, 1, Downloaded from https://chemistry-europe.onlinelibrary.wiley.com/doi/10.1002/batt.202000201 by University of Ulsan, Wiley Online Library on [11/11/2025]. See the Terms and Conditions (https://onlinelibrary.wiley.com/terms-and-conditions) on Wiley Online Library for rules of use; OA articles are governed by the applicable Creative Commons License

thus may provide some hint of their potential capability to host a large amount of discharge products. For example, the relatively large density difference of c-G/hG vs. t-G/hG (1.18 vs. 0.85 g cm^{-3}) is consistent with their sizable difference in full discharge capacity (27 vs 53 mAh cm^{-2}). However, this still does not directly reflect the properties of electrolyte-filled discs. Future studies might include emerging in situ visualization techniques such as high-resolution X-ray micro-tomography, which may provide direct physical information on the air cathodes during battery operation. Chemical factors such as oxygen content might have also contributed, as it appears that larger capacity values of some cells were associated with higher C/O ratios or lower oxygen content (Table 1 and 2). But the presence of some exceptions (such as MWNT-S) strongly suggest that architectural expandability is a descriptor collectively determined by a variety of physical and chemical characteristics of the air cathode.

2.3. Cycling Performance

It has been commonly observed that non-aqueous Li–O_2 batteries with 100% DOD (i.e., fully discharged) are often of poor cyclability because of large-sized discharge products, poor kinetics, and parasitic reactions.[1] With an ultrahigh total carbon mass loading of 10 mg cm^{-2} in this work, attempts to fully charge the Li–O_2 batteries after 100% DOD for all the composite cathodes also consistently resulted in premature cell failure before reaching complete charge (Figure S7). This can be at least partially attributed to the loss of electrical contact of the large, partially discharged Li_2O_2 particles to the substrate upon charging and undesirable solid-electrolyte interface (SEI) formed on Li anode surfaces during deep discharge.

As mentioned earlier, it has been a common practice to curtail the DOD in order to avoid the extreme reaction exertions and therefore to improve the battery reaction reversibility, albeit with a lower achievable capacity. Under this notion, we adopted a protocol in which the cells were first discharged to a maximum of 2000 mAh g_C^{-1} (or 20 mAh cm^{-2}) then cycled at a common curtailed capacity of 500 mAh g_C^{-1} (or 5 mAh cm^{-2}), all at a current density of 0.2 mA cm^{-2}. Note with the different full discharge capacities, the curtailed cycling capacity represent different DODs for the various fillers used. The motivation in using this protocol is to isolate the morphological effects in the air cathode that are only induced by cycling. More specifically, using a sufficiently large first discharge might help ensure the initial establishment of the electrical contact between the discharge product particles and the carbon substrate. Subsequent charge and discharge with reduced depth would result in presumably just the change in the size of the discharge particles without repeatedly removing and re-establishing the substrate-particle electrical contact, thus minimizing potential side effects from different anchoring strengths associated with the various carbon nanomaterial additives.

As shown in Figure 3, the cycling performance of the Li–O_2 batteries with various cathode carbon nanomaterial additives exhibited a drastically different trend from that observed from full discharge studies. With the exception of c-G, all other additives resulted in an improvement in cyclability, in the order of c-G < no additive (hG only) < CB < t-G < MWNT-L < MWNT-S. Interestingly, both types of MWNT additives provided the most improvements in cyclability, while, in stark contrast, their full discharge capacities were among the lowest as discussed above (Figure 2). For example, in comparison to 5 cycles of the neat hG cathode that maintained the curtailed discharge capacity at each cycle, MWNT-S/hG was able to maintain

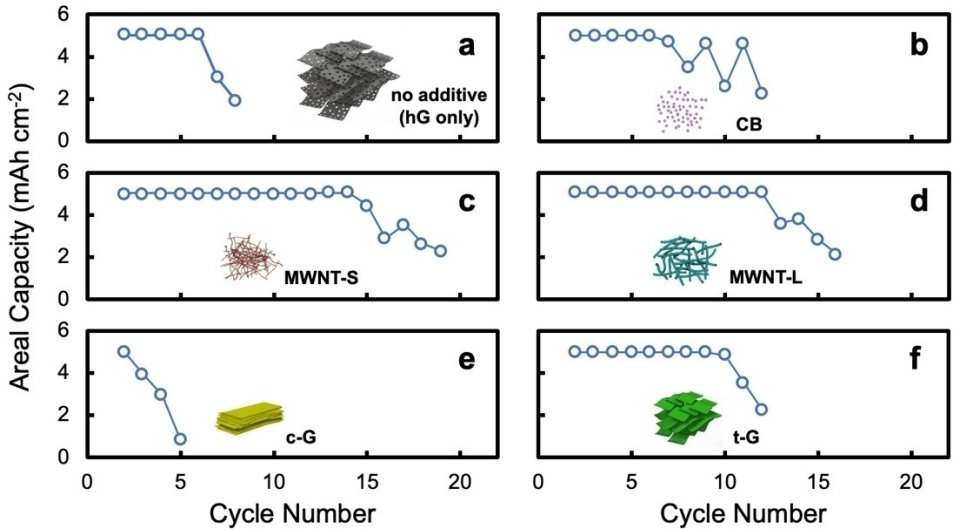

Figure 3. Curtailed cycling performance (in terms of discharge areal capacity) of Li–O_2 batteries with a) a neat hG air cathode and dry-pressed hG composite air cathodes with various carbon nanomaterial additives (additive: hG = 1:5 w/w): b) CB; c) MWNT-S; d) MWNT-L; e) c-G; and () t-G. Current densities were 0.2 mA cm^{-2}. The areal capacity of the first discharge was set at a maximum of 20 mAh cm^{-2} (not shown); the subsequent charge and all cycles were all set at a maximum of 5 mAh cm^{-2}.

© 2020 Wiley-VCH GmbH

25666223, 2021, 1, Downloaded from https://chemistry-europe.onlinelibrary.wiley.com/doi/10.1002/batt.202000201 by University of Ulsan, Wiley Online Library on [11/11/2025]. See the Terms and Conditions (https://onlinelibrary.wiley.com/terms-and-conditions) on Wiley Online Library for rules of use; OA articles are governed by the applicable Creative Commons License

13 cycles, while c-G/hG could not even sustain a full second cycle.

One might argue that the residual metals in the MWNTs (not purified) could help with charge reaction thereby improving cyclability. Several experimental observations are against this argument. First, as discussed earlier, the step cycle experiments with a lower curtailed capacity at different current densities (Figure S3) suggested that all the carbon nanomaterial additives are catalytically equivalent toward both charge and discharge due to the lack of any meaningful overpotential difference. Furthermore, at cycle 5, for example, the charge overpotential (a common indicator of charge catalytic effect) of the air cathode with MWNT-S/hG was even higher than those with both neat hG and G/hG (Figure S8), but the latter two failed earlier.

The different outcome between full discharge and cycling experiments is better seen in Figure 4a, where the cycling performance is reflected in the total output capacity values by summing up capacities of all cycles before dropping below 2.5 mAh cm^{-2} as the cutoff capacity. Such a lack of correlation between the two types of measurements strongly suggest that they are dictated by completely different factors. As discussed in the previous section, the architectural expandability determines the full discharge capacity of the air cathodes. In comparison, as shown in Figure 4b, the air cathodes for curtailed cycling with a reversible capacity of 5 mAh cm^{-2} experience a much smaller volume/thickness change [$\Delta t = 18.5$ ($\Delta V/\Delta V_0$) μm] in comparison to those for full discharge. Therefore, it is understandable that the maximal architectural expandability is not the determining factor for curtailed cycling. Rather, the architectural transformation in curtailed cycling is featured with repeated air cathode volume expansion and contraction, with the extent corresponding to the curtailed capacity. With a relatively small curtailed capacity where the air cathode architecture exhibits only limited volume change, the architectural resilience against the repeated small volume change, or "breathability" (as a reference to animal lungs during respiration), should be the dominant factor.

As shown in Figure 4a, composite air cathodes with both types of MWNT fillers were of the best breathability, providing with up to ~5 times increase in total capacity output with curtailed cycling when compared to that with full discharge. This also suggests that the discharge and charge reactions were reasonably reversible. However, the neat hG and composite air cathodes with both 2D fillers from curtailed cycling provided much smaller improvement over full discharge in total capacity output, suggesting much less reversible reactions. One of the most common failure modes of carbon-based air cathodes is the build-up of side-products that ultimately cover all the active area due to parasitic reactions during charge (such as electrolyte decomposition).[1–3] 2D fillers including both c-G and t-G are structurally similar to the hG matrix. With the dimensional similarity, the inter-sheet interactions might become increasingly significant with building up of the side products during cycling at a curtailed capacity. In comparison, both 0D and 1D fillers, especially the MWNTs, disrupted the restacking characteristics of the hG architectural matrix, providing more accessible void volumes during repeated discharge and making them more resilient in mitigating the negative effects from side product build-up. As shown in Figure S8, the charge overpotentials of the t-G/hG air cathode and the neat hG air cathode increased over repeated cycles, suggesting increasingly inefficient charge reactions. The MWNT-S/hG air cathode, on the other hand, exhibited even lower charge potential at cycle 10 than cycle 5, suggesting

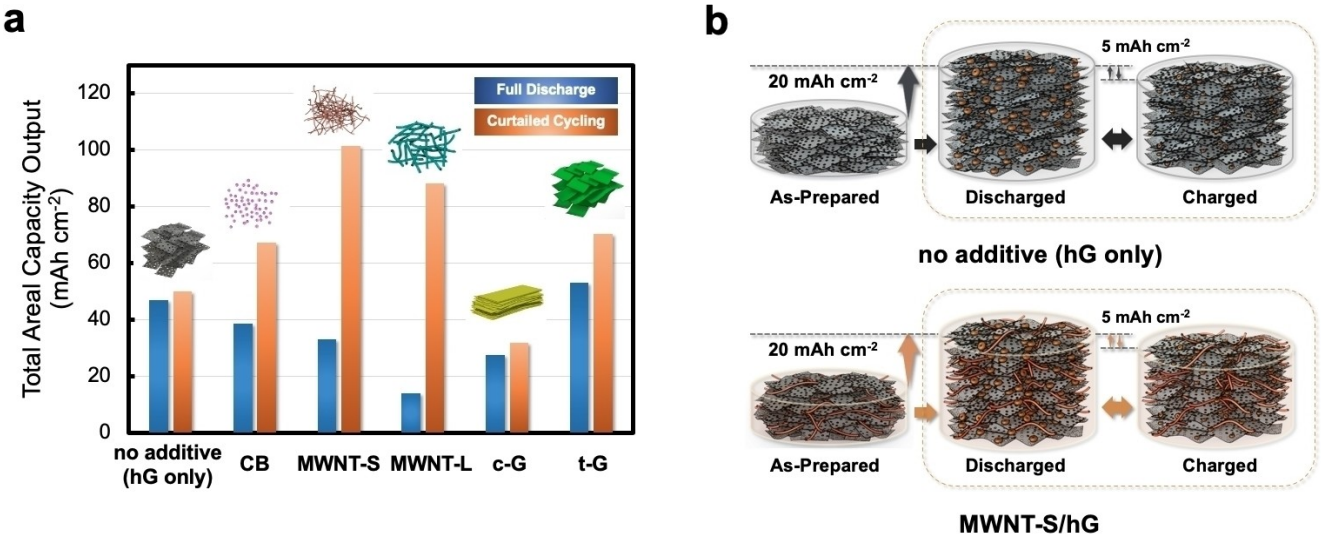

Figure 4. a) A bar chart to compare the total areal capacity output in full discharge (blue) and curtailed cycling (orange) measurements from Li–O_2 batteries with dry-pressed neat hG air cathode (leftmost) and hG-based composite air cathodes with various carbon nanomaterial additives, including (from left to right) CB, MWNT-S, MWNT-L, c-G, and t-G. b) Cartoon illustration (not drawn to scale) showing architectural transformations of a neat hG air cathode (no additive) vs. a MWNT-S/hG composite air cathode from the same test protocol including a first discharge to 20 mAh cm^{-2} followed by curtailed cycling at 5 mAh cm^{-2}. Toroidal shaped Li_2O_2 particles are shown in golden color.

© 2020 Wiley-VCH GmbH

25666223, 2021, 1, Downloaded from https://chemistry-europe.onlinelibrary.wiley.com/doi/10.1002/batt.202000201 by University of Ulsan, Wiley Online Library on [11/11/2025]. See the Terms and Conditions (https://onlinelibrary.wiley.com/terms-and-conditions) on Wiley Online Library for rules of use; OA articles are governed by the applicable Creative Commons License

25666223, 2021, 1, Downloaded from https://chemistry-europe.onlinelibrary.wiley.com/doi/10.1002/batt.202000201 by University of Ulsan, Wiley Online Library on [11/11/2025]. See the Terms and Conditions (https://onlinelibrary.wiley.com/terms-and-conditions) on Wiley Online Library for rules of use; OA articles are governed by the applicable Creative Commons License

favorable, if not improved, charge environment over repeated cycling.

It is expected that the enhancement of such architectural resilience may be further achieved by using catalysts that can improve the battery reactions while suppressing the undesirable side reactions especially during charge. Unlike the architectural expandability, which is mostly structure driven at ultrahigh areal capacity, the air cathode breathability may be more influenced by both chemistry and volume factors. At a low curtailed capacity (e.g., $<1\ mAh\ cm^{-2}$), the volumetric effect is nearly negligible, while the chemistry factor, i.e., the battery reaction efficiency, is predominant as shown in most Li–O_2 battery research thus far with low carbon mass loadings in the air cathodes. However, with the required increase of reversible areal capacity to the range of 10–20 $mAh\ cm^{-2}$ to achieve a competitive cell level specific energy ($>600\ Wh\ kg^{-1}$), the repeated electrode volume change becomes much more prominent [$\Delta t = 35(\Delta V/\Delta V_0)$–$70(\Delta V/\Delta V_0)$ μm], for which the 3-dimensional architecture structure should then be carefully considered. The use of architectural additives thus needs to strike a balance between volume expandability and resilience.

3. Summary and Perspectives

Various carbon nanomaterial additives used in dry-pressed hG-based air cathodes resulted in significantly different full discharge and curtailed cycling properties that do not directly correlate. These additives can be considered catalytically equivalent, but contribute differently to the architecture transformations of the hG host scaffold. For full discharge, most additives reduce the total capacity output compared to the neat hG air cathode. However, for curtailed cycling, the trend almost entirely reverses. We propose that the full discharge capacity of these air cathodes is determined by the architectural volume expandability, which depicts the quasi-slurry, microporous nature of hG-based air cathodes that can withstand extraordinary volume expansion toward ultrahigh areal capacity (up to $>50\ mAh\ cm^{-2}$) while maintaining electrochemical integrity. The curtailed cycling, with much smaller but still significant electrode volume change, was more affected by the air cathode architectural resilience, or "breathability", which may help in negating the detrimental parasitic reactions – not by any increased catalytic nature but by dimensional disruption induced by additives such as carbon nanotubes.

It is important to point out that these emerging concepts such as architectural expandability and breathability are much less relevant for low areal capacity air cathodes with low carbon mass loading that are the most common in the current literature where the electrode surface phenomenon dominates the Li–O_2 battery performance. However, they are critical considerations for the future development of high areal capacity air cathodes for non-aqueous Li–O_2 batteries with practical values. Further improvement in full discharge capacity of air cathodes requires the increase of the amount of electrochemically viable micrometer-sized pores, which corresponds to mass loading increase for expandable platforms such as hG or carbon nanotube films or more effective pre-existing macropores utilization for macroporous hard carbon platforms such as biomass-derived carbon frameworks. In either case, the reduced ion and O_2 availability throughout the entire ultrathick architecture must be effectively dealt with. Although ultrahigh areal capacity has now been achieved in fully discharged Li–O_2 batteries by using high carbon mass loading air cathodes with dry-pressed hG- or carbon nanotube film-based platforms, it remains a grand challenge to increase the reversible fraction of the full capacity while further decreasing the required carbon loading to improve the active material (O_2) utilization. Nevertheless, in the near future, it is imperative for the community to put an emphasis in the Li–O_2 battery research on the cells with reversible areal capacity at least at a meaningful level (at least 5–10 $mAh\ cm^{-2}$), for which the air cathode architectural considerations should be critically evaluated in addition to the various effective heterogeneous and homogeneous catalytic chemistries. Analytical advances in visualization and quantification the in situ 3D morphology change of high areal capacity air cathodes are also in urgent need.

Experimental Section

Materials

Carbon black ("CB", TIMCAL SUPER C45 Conductive Carbon Black, EQ-Lib-SuperC45), large diameter multi-walled carbon nanotubes ("MWNT-L", batch# UK115b, diameter ~20–150 nm), small diameter multi-walled carbon nanotubes ("MWNT-S", 95+%, OD <8 nm), chemically reduced graphene oxide ("c-G", rGO or reduced graphene oxide), and thermally reduced graphene oxide ("t-G", Vor-X graphene; grade: reduced 070; lot: BK-77x) were obtained from MTI Corp., University of Kentucky, Nanostructured & Amorphous Materials, Inc., Carbon Solutions Inc., and Vorbeck Materials, respectively. hG was prepared in a one-step air oxidation procedure by heating a t-G sample to 440 °C and holding for 10 h as previously reported[23] (yield ~88% for this work). Li chips (15.6 mm in diameter; 0.45 mm in thickness; EQ-Lib-LiC45) were purchased from MTI Corp. Lithium bis(trifluoromethane)sulfonimide (LiTFSI; Sigma-Aldrich, 99.95%) and tetraethylene glycol dimethyl ether (TEGDME; Sigma-Aldrich, ≥99%) were purchased from Sigma-Aldrich. TEGDME were dried over freshly regenerated molecular sieves before use. All other materials and chemicals were used as-received.

hG-Based Composite Mixture

In a typical experiment, 20 mg of the respective carbon nanomaterial additive powder and 100 mg hG were loaded in a 20-mL zirconia vial (SPEX CertiPrep, 6.4 cm long, 5.7 cm outer diameter) with two zirconia balls (SPEX CertiPrep, d = 1.3 cm). The vial was subject to mechanical shaking (~1060 back-and-forth cycles per minute, 5.7 cm back-and-forth and 2.5 cm side-to-side movements) for 10 seconds in a SPEX CertiPrep 8000D High-Energy Shaker Mill to yield the respective composite powder mixture.

hG-Based Air Cathodes from Dry-Press

In a typical experiment to fabricate an air electrode with a carbon mass loading of 10 $mg\ cm^{-2}$, a piece of stainless steel (SS) woven

© 2020 Wiley-VCH GmbH

wire mesh (15 mm in diameter; MTI Corp.), ~17–18 mg of neat hG or the hG-based composite mixture, and another piece of similar SS woven wire mesh were sequentially loaded to a SS pressing die (MTI Corp.; Model EQ-Die-15D; 14.85 mm in inner diameter). The die was then placed in a hydraulic press (Carver Hydraulic Unit Model #3925) and applied with a load of ~200 MPa (equivalent to ~8000 lbs). After 10–15 minutes, the die was unloaded, and the pellet was removed from the die to be directly used as air cathode in subsequent Li–O_2 battery assembly. For physical characterizations, freestanding discs of identical compositions were prepared using the same procedure but with two precisely cut Celgard membranes (MTI Corp.) as separation layers instead of the wire meshes. The plastic membranes were peeled off after the pellets were formed.

Li–O_2 Battery Assembly

The Li–O_2 batteries were assembled in the format of CR2032 coin cells in an Ar-filled glove box. Because the cathode cap is perforated, the assembly process started with the anode cap to avoid losing electrode material and electrolyte. Note the assembly for Li-ion battery coin cells conventionally starts with the cathode cap instead. In a typical process, a piece of Li chip was placed in a SS anode cap, followed by addition of 90 μL of the electrolyte (1 M LiTFSI in TEGDME). A piece of glass fiber membrane (19 mm in diameter; Whatman) as a separator was then placed on top of the wet Li chip to cover the entire anode cap opening. Another 90 μL of electrolyte was added to wet the glass fiber membrane. The hG-based air cathode was then centered on top of the membrane, followed by the addition of another 90 μL of electrolyte to completely wet the cathode. After applying electrolyte, the cathode became swollen, which is typical for hG-based air cathodes. After placing a SS wave spring (MTI Corp.) on top of the wet air cathode, a perforated cathode cap (MTI Corp.) was carefully placed on the very top and gently pushed down to encase the anode cap. The entire assembly was placed in a hydraulic crimping device (MTI Model MSK-110) and crimped at a pressure of ~5.5 MPa (or ~800 psi) into a functional coin cell battery.

Li–O_2 Battery Testing

The Li–O_2 coin cells were tested in a custom-built air-tight box with continuous flow (30–50 mL min^{-1}) of pure O_2 using either a multi-channel battery analyzer (MTI Corporation; Model BST8-MA) or a multi-channel electrochemical station (Bio-Logic; Model VMP3). The discharge and charge voltage limits were set at 2.0 and 4.5 V, respectively. Areal current densities of 0.1, 0.2, and 0.5 mA cm^{-2} were calculated based on the geometrical area of the as-prepared air cathode (1.73 cm^2), with the actual currents being 0.173, 0.346, and 0.865 mA, respectively. Electrochemical impedance spectroscopy (EIS) was also conducted on the BioLogic VMP-3 electrochemical station. EIS was measured at the open circuit potential (typically in the range of 3.0–3.4 V) in the frequency range of 1 MHz to 0.01 Hz with an amplitude of 10 mV and 10 points measured per decade.

Other Measurements

Scanning electron microscopy (SEM) images were acquired using a Hitachi S-5200 field emission SEM (FE-SEM) system at an acceleration voltage of 30 keV. X-ray photoelectron spectroscopy (XPS) data were acquired using a custom-built system consisting of a DESA-100 analyzer (STAIB Instruments) and a monochromatic Al K-alpha X-ray (1.486 keV photon energy) source operated at 15 keV. Nitrogen adsorption-desorption isotherms and the corresponding Brunauer-Emmett-Teller (BET) surface area values were estimated from N_2 adsorption/desorption isotherms acquired on a Quantachrome Nova 2200e Surface Area and Pore Size Analyzer system using a 9 mm cell. Surface DC conductivity was measured with a 4-point probe system (Signatone, QuadPro Resistivity Wafer Mapping System) at room temperature.

Acknowledgements

Financial support from the NASA Langley Internal Research and Development (IRAD) Program and Center Innovation Fund (CIF) is gratefully acknowledged. We also thank the NASA Interns, Fellows, and Scholars (NIFS) Program, which supported L.G. and C.P.-R. as student interns at the NASA Langley Research Center.

Conflict of Interest

The authors declare no conflict of interest.

Keywords: Li–O_2 batteries · air cathode · electrode architecture · high areal capacity · holey graphene

[1] a) J. Lu, L. Li, J.-B. Park, Y.-K. Sun, F. Wu, K. Amine, *Chem. Rev.* **2014**, *114*, 5611–5640; b) N. Feng, P. He, H. Zhou, *Adv. Energy Mater.* **2016**, *6*, 1502303; c) W.-J. Kwak, Rosy, D. Sharon, C. Xia, H. Kim, L. R. Johnson, P. G. Bruce, L. F. Nazar, Y.-K. Sun, A. A. Frimer, M. Noked, S. A. Freunberger, D. Aurbach, *Chem. Rev.* **2020**, *14*, 6626–6683.

[2] a) Y.-C. Lu, B. M. Gallant, D. G. Kwabi, J. R. Harding, R. R. Mitchell, M. S. Whittingham, Y. Shao-Horn, *Energy Environ. Sci.* **2013**, *6*, 750–768; b) H.-D. Lim, B. Lee, Y. Bae, H. Park, Y. Ko, H. Kim, J. Kim, K. Kang, *Chem. Soc. Rev.* **2017**, *46*, 2873–2888; c) F. Li, J. Chen, *Adv. Energy Mater.* **2017**, *7*, 1602934; d) Z. Lyu, Y. Zhou, W. Dai, X. Cui, M. Lai, L. Wang, F. Huo, W. Huang, Z. Hu, W. Chen, *Chem. Soc. Rev.* **2017**, *46*, 6046–6072; e) C. Shu, J. Wang, J. Long, H.-K. Liu, S.-X. Dou, *Adv. Mater.* **2019**, *31*, 1804587.

[3] a) J. Xu, J. Ma, Q. Fan, S. Guo, S. Dou, *Adv. Mater.* **2017**, *29*, 1606454; b) Z. Chang, J. Xu, X. Zhang, *Adv. Energy Mater.* **2017**, *7*, 1700875; c) K.-X. Wang, Q.-C. Zhu, J.-S. Chen, *Small* **2018**, *14*, 1800078; d) D. Wang, X. Mu, P. He, H. Zhou, *Mater. Today* **2019**, *26*, 87–99; e) L. Ma, T. Yu, E. Tzoganakis, K. Amine, T. Wu, Z. Chen, J. Lu, *Adv. Energy Mater.* **2018**, *8*, 1800348; f) M. Balaish, J.-W. Jung, I.-D. Kim, Y. Ein-Eli, *Adv. Funct. Mater.* **2020**, *30*, 1808303; g) J.-W. Jung, S.-H. Cho, J. S. Nam, I.-D. Kim, *Energy Storage Mater.* **2020**, *24*, 512–528.

[4] D. Geng, N. Ding, T. S. A. Hor, S. W. Chien, Z. Liu, D. Wuu, X. Sun, Y. Zong, *Adv. Energy Mater.* **2016**, *6*, 1502164.

[5] a) H. Kim, H.-D. Lim, J. Kim, K. Kang, *J. Mater. Chem. A* **2014**, *2*, 33–47; b) Y. Tu, D. Deng, X. Bao, *J. Energy Chem.* **2016**, *25*, 957–966; c) H. Woo, J. Kang, J. Kim, C. Kim, S. Nam, B. Park, *Electr. Mater. Lett.* **2016**, *12*, 551–567; d) J. Xiao, D. Mei, X. Li, W. Xu, D. Wang, G. L. Graff, W. D. Bennett, Z. Nie, L. V. Saraf, I. A. Aksay, J. Liu, J.-G. Zhang, *Nano Lett.* **2011**, *11*, 5071–5078; e) J. Kang, O. L. Li, N. Saito, *J. Power Sources* **2014**, *261*, 156–161; f) Y. Li, J. Wang, X. Li, D. Geng, R. Li, X. Sun, *Chem. Commun.* **2011**, *47*, 9438–9440; g) H.-D. Lim, K.-Y. Park, H. Song, E. Y. Jang, H. Gwon, J. Kim, Y. H. Kim, M. D. Lima, R. O. Robles, X. Lepro, R. H. Baughman, K. Kang, *Adv. Mater.* **2013**, *25*, 1348–1352; h) R. A. Wong, A. Dutta, C. Yang, K. Yamanaka, T. Ohta, A. Nakao, K. Waki, H. R. Byon, *Chem. Mater.* **2016**, *28*, 8006–8015.

[6] M. Hagen, D. Hanselmann, K. Ahlbrecht, R. Maça, D. Gerber, J. Tübke, *Adv. Energy Mater.* **2015**, *5*, 1401986.

[7] M. M. O. Thotiyl, S. A. Freunberger, Z. Peng, P. G. Bruce, *J. Am. Chem. Soc.* **2013**, *135*, 494–500.

[8] M. Noked, M. A. Schroeder, A. J. Pearse, G. W. Rubloff, S. B. Lee, *J. Phys. Chem. Lett.* **2016**, *7*, 211–215.

[9] Y. Lin, B. Moitoso, C. Martinez-Martinez, E. D. Walsh, S. D. Lacey, J.-W. Kim, L. Dai, L. Hu, J. W. Connell, *Nano Lett.* **2017**, *17*, 3252–3260.

© 2020 Wiley-VCH GmbH

25666223, 2021, 1, Downloaded from https://chemistry-europe.onlinelibrary.wiley.com/doi/10.1002/batt.202000201 by University of Ulsan, Wiley Online Library on [11/11/2025]. See the Terms and Conditions (https://onlinelibrary.wiley.com/terms-and-conditions) on Wiley Online Library for rules of use; OA articles are governed by the applicable Creative Commons License

[10] a) S. D. Lacey, E. D. Walsh, E. Hitz, J. Dai, J. W. Connell, L. Hu, Y. Lin, *Nano Energy* **2017**, *31*, 386–392; b) Y. Lin, C. Martinez-Martinez, J.-W. Kim, J. W. Connell, *J. Electrochem. Soc.* **2020**, *167*, 080522.
[11] H.-J. Shin, W.-I. Kwak, D. Aurbach, Y.-K. Sun, *Adv. Funct. Mater.* **2017**, *27*, 1605500.
[12] A. Nomura, K. Ito, Y. Kubo, *Sci. Rep.* **2017**, *7*, 45596.
[13] a) Y. J. Lee, S. H. Park, S. H. Kim, Y. Ko, K. Kang, Y. J. Lee, *ACS Catal.* **2018**, *8*, 2923–2934; b) S. H. Park, Y. J. Cheon, Y. J. Lee, K. H. Shin, Y. Y. Hwang, Y. S. Jeong, Y. J. Lee, *ACS Appl. Mater. Interfaces.* **2019**, *11*, 30872–30879.
[14] S. Xu, Y. Yao, Y. Guo, X. Zeng, S. D. Lacey, H. Song, C. Chen, Y. Li, J. Dai, Y. Wang, Y. Chen, B. Liu, K. Fu, K. Amine, J. Lu, L. Hu, *Adv. Mater.* **2017**, *30*, 1704907.
[15] S. D. Lacey, D. J. Kirsch, Y. Li, J. T. Morgenstern, B. C. Zarket, Y. Yao, J. Dai, L. Q. Garcia, B. Liu, T. Gao, S. Xu, S. R. Raghavan, J. W. Connell, Y. Lin, L. Hu, *Adv. Mater.* **2018**, *30*, 1705651.
[16] H. Song, S. Xu, Y. Li, J. Dai, A. Gong, M. Zhu, C. Zhu, C. Chen, Y. Chen, Y. Yao, B. Liu, J. Song, G. Pastel, L. Hu, *Adv. Energy Mater.* **2018**, *8*, 1701203.
[17] M. Hayashi, S. Sakamoto, M. Nohara, M. Iwata, T. Komatsu, *Electrochemistry* **2018**, *86*, 333–338.
[18] H. C. Lee, J. O. Park, M. Kim, H. J. Kwon, J.-H. Kim, K. H. Choi, K. Kim, D. Im, *Joule* **2019**, *3*, 542–556.
[19] P. Wunderlich, J. Kupper, U. Simon, *Materials* **2020**, *13*, 43.
[20] S. Zhao, L. Zhang, G. Zhang, H. Sun, J. Yang, S. Lu, *J. Energy Chem.* **2020**, *45*, 74–82.
[21] X. Han, Z. Yang, B. Zhao, S. Zhu, L. Zhou, J. Dai, J.-W. Kim, B. Liu, J. W. Connell, T. Li, B. Yang, Y. Lin, L. Hu, *ACS Nano* **2017**, *11*, 3189–3197.
[22] a) Y. Lin, Y. Liao, Z. Chen, J. W. Connell, *Mater. Res. Lett.* **2017**, *5*, 209–234; b) Z. Chen, X. An, L. Dai, Y. Xu, *Nano Energy* **2020**, *73*, 104762; c) Y. Tao, Z.-Y. Sui, B.-H. Han, *J. Mater. Chem. A* **2020**, *8*, 6125–6143.
[23] a) X. Han, M. R. Funk, F. Shen, Y.-C. Chen, Y. Li, C. J. Campbell, J. Dai, X. Yang, J.-W. Kim, Y. Liao, J. W. Connell, V. Barone, Z. Chen, Y. Lin, L. Hu, *ACS Nano* **2014**, *8*, 8255–8265; b) Y. Lin, X. Han, C. J. Campbell, J.-W. Kim, B. Zhao, W. Luo, J. Dai, L. Hu, J. W. Connell, *Adv. Funct. Mater.* **2015**, *25*, 2920–2927.
[24] a) D. Chen, H. Feng, J. Li, *Chem. Rev.* **2012**, *112*, 6027–6053; b) C. K. Chua, M. Pumera, *Chem. Soc. Rev.* **2014**, *43*, 291–312.
[25] a) H. C. Schniepp, J.-L. Li, M. J. McAlister, H. Sai, M. Herrera-Alonso, D. H. Adamson, R. K. Prud'homme, R. Car, D. A. Saville, I. A. Aksay, *J. Phys. Chem. B* **2006**, *110*, 8535–8539; b) Y.-Y. Peng, Y.-M. Liu, J.-K. Chang, C.-H. Wu, M.-D. Ger, N.-W. Pu, C.-L. Chang, *Carbon* **2016**, *81*, 347–356.
[26] D. J. Kirsch, S. D. Lacey, Y. Kuang, G. Pastel, H. Xie, J. W. Connell, Y. Lin, L. Hu, *ACS Appl. Energy Mater.* **2019**, *2*, 2990–2997.
[27] a) T. Zhang, H. Matsuda, H. Zhao, *ChemSusChem* **2014**, *7*, 2845–2852; b) C. Shu, B. Li, B. Zhang, D. Su, *ChemSusChem* **2015**, *8*, 3973–3976; c) W. Wan, X. Zhu, X. He, Y. Wang, Y. Yan, Y. Wu, Z. Lu, *J. Electrochem. Soc.* **2018**, *165*, A1741–A1745; d) Y. Xiao, F. Du, C. Hu, Y. Ding, Z. L. Wang, A. Roy, L. Dai, *ACS Energy Lett.* **2020**, *5*, 916–921.
[28] Y. Lin, K. J. Jones, L. C. Greenburg, J.-W. Kim, L. Hu, J. W. Connell, *Batteries & Supercaps* **2019**, *2*, 774–783; Supercaps **2019**, 2, 774–783.

Manuscript received: August 26, 2020
Revised manuscript received: September 21, 2020
Accepted manuscript online: September 22, 2020
Version of record online: October 13, 2020

© 2020 Wiley-VCH GmbH

25666223, 2021, 1, Downloaded from https://chemistry-europe.onlinelibrary.wiley.com/doi/10.1002/batt.202000201 by University of Ulsan, Wiley Online Library on [11/11/2025]. See the Terms and Conditions (https://onlinelibrary.wiley.com/terms-and-conditions) on Wiley Online Library for rules of use; OA articles are governed by the applicable Creative Commons License